Ice chemistry of acetaldehyde reveals competitive reactions in the first step of the Strecker synthesis of alanine: formation of HO-CH(CH3)-NH2 vs. HO-CH(CH3)-CN

Aurélien Fresneau, Grégoire Danger, Albert Rimola, Fabrice Duvernay, Patrice Theulé, Thierry Chiavassa

Monthly Notices
of the
ROYAL ASTRONOMICAL SOCIETY

MNRAS **451,** 1649–1660 (2015) doi:10.1093/mnras/stv1033

Ice chemistry of acetaldehyde reveals competitive reactions in the first step of the Strecker synthesis of alanine: formation of HO–CH(CH_3)–NH_2 vs. HO–CH(CH_3)–CN

Aurélien Fresneau,[1] Grégoire Danger,[1]★ Albert Rimola,[2] Fabrice Duvernay,[1] Patrice Theulé[1] and Thierry Chiavassa[1]

[1]*Aix-Marseille Université, PIIM UMR-CNRS 7345, F-13397 Marseille, France,*
[2]*Departament de Quimica, Universitat Autonoma de Barcelona, E-08193 Bellaterra, Spain*

Accepted 2015 May 5. Received 2015 April 17; in original form 2015 February 18

ABSTRACT

The understanding of compound formation in laboratory simulated astrophysical environments is an important challenge in obtaining information on the chemistry occurring in these environments. We here investigate by means of both laboratory experiments and quantum chemical calculations the ice-based reactivity of acetaldehyde (CH_3CHO) with ammonia (NH_3) and hydrogen cyanide (HCN) in excess of water (H_2O) promoted by temperature. A priori, this study should give information on alanine ($_2$HN–CH(CH_3)–COOH) formation (the simplest chiral amino acid detected in meteorites), since these reactions concern the first steps of its formation through the Strecker synthesis. However, infrared spectroscopy, mass spectrometry with $HC^{14}N$ or $HC^{15}N$ isotopologues and B3LYP-D3 results converge to indicate that an H_2O-dominated ice containing CH_3CHO, NH_3 and HCN not only leads to the formation of α-aminoethanol ($_2$HN–CH(CH_3)–OH, the product compound of the first step of the Strecker mechanism) and its related polymers ($_2$HN–(CH(CH_3)–O)$_n$–H) due to reaction between CH_3CHO and NH_3, but also to the 2-hydroxypropionitrile (HO–CH(CH_3)–CN) and its related polymers (H–(O–CH(CH_3))$_n$–CN) from direct reaction between CH_3CHO and HCN. The ratio between these two species depends on the initial NH_3/HCN ratio in the ice. Formation of α-aminoethanol is favoured when the NH_3 concentration is larger than HCN. We also show that the presence of water is essential for the formation of HO–CH(CH_3)–CN, contrarily to $_2$HN–CH(CH_3)–OH whose formation also takes place in absence of H_2O ice. As in astrophysical ices NH_3 is more abundant than HCN, formation of α-aminoethanol should consequently be favoured compared to 2-hydroxypropionitrile, thus pointing out α-aminoethanol as a plausible intermediate species for alanine synthesis through the Strecker mechanism in astrophysical ices.

Key words: astrochemistry – molecular data – molecular processes – comets: general.

1 INTRODUCTION

Numerous amino acids have been detected in meteorites (Burton et al. 2012). The chemical pathways that lead to their formation are not fully understood (Elsila et al. 2007), although the Strecker synthesis (Strecker 1854; Kendall & McKenzie 1929) is often presented as the main reaction channel (Lerner & Cooper 2005). This synthesis involves the reaction of aldehydes or ketones (CR_1R_2=O) with ammonia (NH_3) and hydrogen cyanide (HCN). The first step is the addition of NH_3 to an aldehyde/ketone leading to the formation of the corresponding aminoalcohol ($_2$HN–CR_1R_2–OH). This compound is then dehydrated to form an imine (CR_1R_2=NH), which subsequently react with HCN/$^-$CN to form an aminonitrile ($_2$HN–CR_1R_2–CN). Finally, the nitrile is hydrated in two steps leading to the formation of the corresponding amino acid ($_2$HN–CR_1R_2–COOH). These successive reactions can occur inside asteroids if conditions allow the formation of an aqueous liquid phase. Isotopic analyses of meteoritic amino acids have shown that isotopic variations are observed between amino acids (Burton et al. 2012), which suggest that amino acids can be formed from different reservoirs of precursors and/or in different environments.

Laboratory experiments have shown that several steps of the Strecker reaction can occur in conditions simulating interstellar or cometary ices. In such cases, reactions do not occur in liquid phase, but rather in solid phase at low pressure (10^{-9} mbar)

* E-mail: gregoire.danger@univ-amu.fr

and at temperatures ranging from 20 to 300 K. It has been experimentally demonstrated that NH_3 reacts at low temperature (50–80 K) with formaldehyde (CH_2=O) and acetaldehyde (CH_3CHO) to form aminomethanol ($_2$HN–CH_2–OH) (Bossa et al. 2009) and α-aminoethanol ($_2$HN–CH(CH_3)–OH) (Duvernay et al. 2010), respectively, both in the presence and absence of H_2O in the ice mixtures. In contrast, reaction of acetone ((CH_3)$_2$CO) with NH_3 to form 2-aminoisopropan-2-ol ($_2$HN–C(CH_3)$_2$–OH) is only possible if H_2O is present, since it traps NH_3 and acetone allowing them to collect enough thermal energy for the reaction to properly proceed (Fresneau et al. 2014). Larger steric hindrances around the carbonyl of the aldehyde/ketone functionalities induce an increase of the activation energies of these reactions. These aminoalcohols can then be transformed into their corresponding imines in the presence of formic acid (HCOOH) (Vinogradoff et al. 2012b), which catalyses the dehydration process. For CH_2O, the imine (CH_2NH) reacts with [NH_4^+ $^-$CN] forming aminoacetonitrile (Danger et al. 2011). However, the formation of glycine ($_2$HN–CH_2–COOH) from aminoacetonitrile does not occur in conditions simulating astrophysical ices (Rimola, Sodupe & Ugliengo 2010; Borget et al. 2012).

The whole Strecker synthesis from aldehydes/ketones, NH_3, HCN, H_2O and HCOOH has not yet been tested experimentally in conditions simulating astrophysical ices. The main problem resides in the characterization of aminonitriles because of the competing reactions that yields the formation of hydroxynitriles (HO–R_1CR_2–CN). These compounds are formed by the addition of $^-$CN to aldehydes/ketones. In the case of CH_2O, it has been shown that hydroxyacetonitrile (HO–CH_2–CN) forms either from an HCN/H_2O ice (Danger et al. 2014), H_2O catalysing the reaction or from an NH_3/HCN ice (Danger et al. 2012), NH_3 here being the catalyst.

In this work, we investigate on the competition between formation of 2-hydroxypropionitrile (HO–HC(CH_3)–CN) and α-aminoethanol ($_2$HN–HC(CH_3)–OH) in simulated astrophysical ices by reaction of acetaldehyde (CH_3CHO) with HCN and NH_3, respectively, paying special attention on the role of water. For this purpose, we used infrared spectroscopy and mass spectrometry associated with isotope labelling for product characterization, and quantum chemical calculations to obtain information on the mechanistic and energetic information of these reactions.

2 METHODS

2.1 Experimental set-up and reactant syntheses

Potassium cyanide (KC^{14}N/ KC^{15}N) and acetaldehyde (CH_3CHO) were purchased from Sigma Aldrich, stearic acid from Fluka analytical and ammonia (NH_3) (99.9 per cent purity) from Air Liquide. Water (H_2O) was distilled in the laboratory. The hydrogen cyanide (HCN) gas used in these experiments was synthesized directly in a Pyrex line at 10^{-3} mbar using the protocol described by Gerakines, Moore & Hudson (2004).

All experiments were performed with the AHIIA system (Analyses from the Heating of Interstellar Ices Analogs), which consists of a high vacuum chamber presenting a pressure of 5×10^{-9} mbar at 295 K and 10^{-9} mbar at 20 K. The gaseous mixture was deposited at a rate of 6×10^{-1} molecules min^{-1} on a copper-plated surface kept at 20 K with a model 21 CTI cold head. The warming of the ice mixture was performed at a heating rate of 4 K min^{-1} using a resistive heater along with a Lakeshore model 331 temperature controller. The infrared spectra of the sample were recorded in reflection absorption mode between 4000 and 600 cm^{-1} using a Brucker Tensor 27 fourier transform infrared spectroscopy (FTIR) spectrometer with an Mercury Cadmium Telluride (MCT) detector. Each spectrum was averaged over one hundred scans with a 1 cm^{-1} resolution. Mass was monitored using an Residual Gas Analyzer (RGA) quadrupole mass spectrometer (MKS Microvision-IP plus) as the products were desorbed during the controlled temperature ramp. The ionization source was a 70 eV impact electronic source and the mass spectra were recorded between 1 and 100 amu in a full scan (Danger et al. 2014).

For the quantitative estimations of the relative amount of H_2O, NH_3, HCN or CH_3CHO in the ice, the following band strengths were used: for HCN ν_{CN} at 2085 cm^{-1} with 5.1×10^{-18} cm molecule^{-1} (Bernstein, Sandford & Allamandola 1997), for CH_3CHO δ_{CH} at 1494 cm^{-1} with 3.9×10^{-18} cm molecule^{-1} (Schutte, Allamandola & Sandford 1993), for H_2O ν_{OH} at 3250 cm^{-1} with 2×10^{-16} cm molecule^{-1} (Gerakines et al. 1995) and for NH_3 ω_{NH} at 1070 cm^{-1} 1.3×10^{-17} cm molecule^{-1}.

As the products formed during the present experiments are more refractory than water, they tend to stick on the sample holder during the water desorption (around 180 K) and remain on it above 180 K. In order to obtain a clear product characterization, we cleaned the sample by warming the sample holder to 185 K to desorb water. The sample holder containing the more refractory compounds was then cooled down to 100 K (sufficiently far from the maximum desorption temperature of the product, while limiting the time for cooling the sample holder). A 4 K min^{-1} ramp was then applied while the ion current was recorded to obtain a full temperature programmed desorption (TPD) of the refractory compounds.

2.3 Computational details

All calculations devoted to calculate the potential energy surfaces (PESs) of the ice reactions were performed using the GAUSSIAN09 package program (Frisch et al. 2013). The structure of each stationary point was fully optimized using the B3LYP-D3 method, which includes an empirical a posteriori correction term proposed by Grimme (2010) to account for dispersion interactions (missed in the pure B3LYP; Lee, Yang & Parr 1988; Becke 1993) density functional method), with the standard 6–311++G(d,p) basis set. All structures were characterized by the analytical calculation of the harmonic frequencies as minima (reactants, intermediates and products) and saddle points (transition states). For some difficult cases, intrinsic reaction coordinate calculations at the same level of theory were carried out to ensure that a given transition structure connects the expected reactants and products. The free energies calculated at different temperatures were obtained by computing the thermochemical corrections to the energy values using the standard harmonic oscillator formulae (McQuarrie 1986) computed at B3LYP/6–31 + G(d,p).

The theoretical simulation of the infrared spectra of an amorphous ice consisting of a mixture of H–(O–CH(CH_3))$_n$–CN, n = 1–3, was done in a two-step procedure. The first step was the execution of classical molecular dynamics (MD) simulations of a large cluster model of 46 molecules to obtain a preliminary amorphous structure of the ice. These MD simulations were carried out in an (N, V, T) ensemble at T = 300 K with the MMF94 classical force field as implemented in the CHEMBIO3D ULTRA program. The obtained structure was then converted in a 3D periodic system in a cubic unit system with 15 Å of length and fully optimized (both internal atomic positions and lattice unit cell parameters) using the CRYSTAL09 code (Dovesi et al. 2009). The final optimized structure of this ice model is shown in Fig. 1. This ice was then used to simulate its infrared spectrum. The geometry optimization and the simulation of the

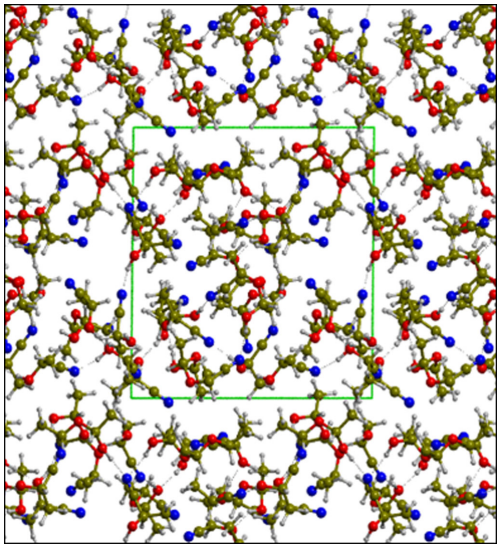

Figure 1. PBE-optimized structure of an amorphous ice model consisting of a mixture of H–(O–CH(CH_3))$_n$–CN, $n = 1$–3.

infrared spectra was carried out using the PBE (Perdew, Burke & Ernzerhof 1996) density functional with a double-ζ basis set.

3 RESULTS

Here, we performed experiments on reactivity between hydrogen cyanide (HCN) and acetaldehyde (CH_3CHO). Ices containing only CH_3CHO:HCN or CH_3CHO:H_2O do not show reactivity. The reactivity of CH_3CHO with NH_3 in diluted conditions has already been studied (Duvernay et al. 2010), but here new investigations are presented, in which the CH_3CHO dilution in the initial ice and its implication on the residue composition is considered.

3.1 Reactivity between HCN and CH_3CHO in an H_2O matrix

Investigations on reactivity between formaldehyde (CH_2O) and HCN have shown that the reaction of HCN with CH_2O can only occur in the presence of H_2O (Fresneau et al. 2014). In this case, H_2O serves to activate HCN, which then reacts with CH_2O, leading to the formation of hydroxyacetonitrile ($HOCH_2CN$) and its related oligomers (H–(O–CH_2)$_n$–CN).

Based on these results, the reactivity of CH_3CHO with HCN was investigated. Similarly to the case of CH_2O, without H_2O, the reaction of HCN with CH_3CHO does not occur. Therefore, H_2O was added to the deposited ice. Fig. 2(A) shows the spectra of two H_2O:HCN:CH_3CHO ices deposited at 20 K in a 1:0.5:0.7 ratio, with $HC^{14}N$ or $HC^{15}N$. The $C^{15}N$ stretching mode presents a shift of 30 cm^{-1} towards lower wavenumbers compared to the $C^{14}N$ stretching mode at 2090 cm^{-1}. The deposit only presents infrared features of H_2O, HCN and CH_3CHO, implying that reactivity does not occur during the deposition or in the solid phase at this temperature. These ices are then warmed at 4 K min^{-1}. Due to the presence of H_2O, it is difficult to monitor the appearance of new infrared bands during the warming period. However, when all reactants have desorbed from the sample holder (210 K), new infrared bands are observed (Fig. 2(B) after cooling down the sample holder to 100 K) meaning that a reaction occurs in the presence of H_2O during the warming-up. However, it is currently difficult to estimate the temperature at which this reaction starts due to the presence of H_2O that masks

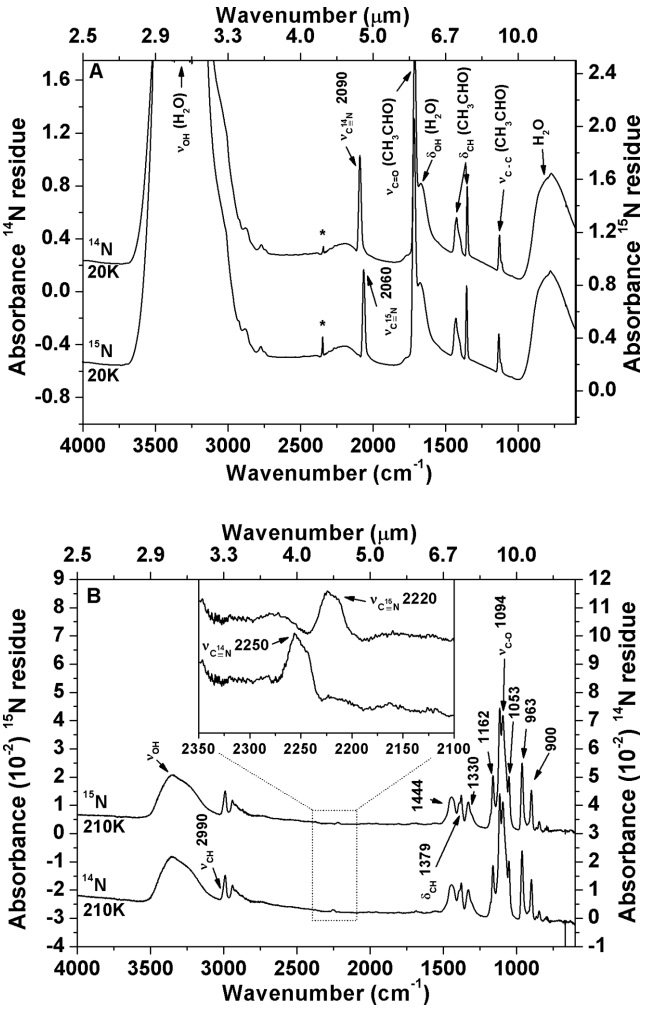

Figure 2. (A) Infrared spectra of H_2O:$HC^{14}N$:CH_3CHO and H_2O:$HC^{15}N$:CH_3CHO mixtures deposited at 20 K in a 1:0.5:0.7 ratio and (B) infrared spectra at 210 K of residues coming from the warming of the ices previously formed at 20 K. Some characteristic bands are displayed and the band marked with $*$ corresponds to CO_2 contamination.

all infrared bands of the new product. In Section 3.3, quantum calculations will give information on reaction constants.

The residue formed from an initial $HC^{14}N$-containing ice presents a band at 2250 cm^{-1}, which is shifted to 2220 cm^{-1} for an initial ice with $HC^{15}N$ as shown in the inset of Fig. 2(B). This means that molecules formed during the warming include a CN moiety, which is consistent with an incorporation of HCN on CH_3CHO. A large band is also observed at 3250 cm^{-1}, which can correspond to the stretching mode of a hydroxyl group. Other bands are present at 1444, 1379, 1330, 1162, 1094, 1053, 963 and 900 cm^{-1}. All these features fit well with those of a hydroxynitrile, as those observed in $HOCH_2CN$ (Danger et al. 2014). To strengthen this infrared attribution, mass spectra of each residue were monitored during their warming from 100 to 250 K. The corresponding mass spectra at 215 K are displayed in Fig. 3 for the ^{14}N and ^{15}N residues. In each case, molecular ions are not observed (m/z 71 and 72 for ^{14}N and ^{15}N isotopologues, respectively). However, ions presenting a loss of one hydrogen are detected at m/z 70 and 71 for ^{14}N and ^{15}N isotopologues, respectively, which is confirmed by the NIST Chemistry Book

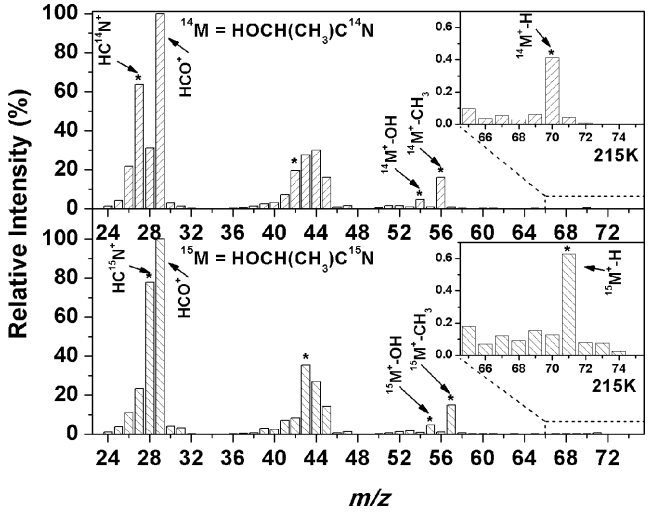

Figure 3. Mass spectra obtained at 215 K during the warming of residues from 100 to 250 K, and coming from an ice containing H_2O:$HC^{14}N$:CH_3CHO or H_2O:$HC^{15}N$:CH_3CHO (infrared spectra of residues are displayed in Fig. 2B). The shift of the various fragments due to ^{15}N is observed and noted by ∗. M–X indicates that the molecular ion lost one X chemical group (see text for fragments labelling).

(http://webbook.nist.gov/cgi/cbook.cgi?ID=C78977&Units=SI&Mask=200#Mass-Spec). The mass shift between these two residues demonstrates that a CN moiety is present on these residues. Furthermore, other characteristic fragments are observed, including fragments presenting a loss of CH_3 or OH (M^+–CH_3 and M^+–OH, respectively, see Fig. 3). All these observations firmly point out that the products remaining on the sample holder after the reactant desorption contains chemical moieties specific of hydroxynitrile.

The ^{14}N-bearing residue was further compared with an $HOCH(CH_3)CN$ standard chemical product and with the simulated at a quantum chemical level (Fig. 4A). In all the spectra, –OH and –CN moieties are present at 3291 and at 2250 cm^{-1}, respectively, confirming that the residue incorporates these two chemical functionalities. Both in the residue and in the standard, asymmetric and symmetric stretching modes of the $–CH_3$ group are found at 2992 and at 2940 cm^{-1}, respectively.

Our residue is thus a combination of $–CH_3$, –OH and –CN chemical groups similar to the $HOCH(CH_3)CN$ standard. By comparing the experimental spectra of the residue with the standard, however, the relative intensities between the $–CH_3$, –OH and –CN groups are different. The relative intensities of OH/CH_3 and CN/CH_3 are lower in the residue than in the standard. These variations can be explained by the presence of a small amount of polymers (see mass spectrum on Fig. 4C). When the polymer length of $H–(O–CH(CH_3))_n–CN$ increases, the relative intensity between bands associated with its chain ends (–OH and –CN) and those of its repetitive unit $–O–CH(CH_3)–$ decreases because the number of the chain ends remains constant whereas the number of the repetitive units increases. This was already observed in the reaction between HCN and CH_2O in a water ice (Danger et al. 2014), and for CH_2NH with NH_3/HCN (Danger et al. 2011). The presence of polymers is also supported by the presence of bands at lower wavenumbers. Although the infrared spectra topology is similar, some bands are present in the residue and not in the standard. This difference is particularly visible in the range 1500–850 cm^{-1}. For instance, a band at 963 cm^{-1} is only present in the residue (noted by ∗ on Fig. 4A).

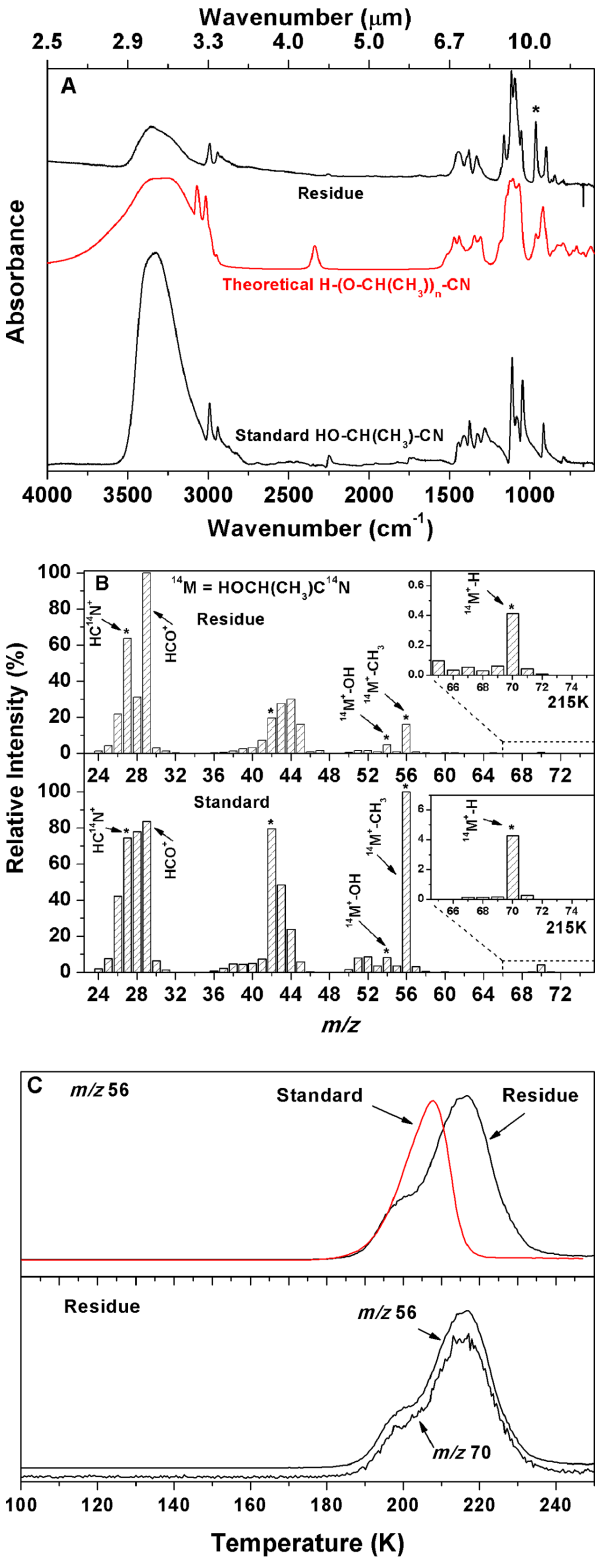

Figure 4. Infrared spectrum (A) of ^{14}N residue (reproduced from Fig. 1B) compared to $HOCH(CH_3)C^{14}N$ standard and $H–(O–CH(CH_3))_n–C^{14}N$ theoretical spectrum (red spectrum). (B) Mass spectrum of ^{14}N residue (reproduced from Fig. 3) compared to $HOCH(CH_3)C^{14}N$ standard. (C) TPD profiles comparisons of ion *m/z* 56 for standard $HOCH(CH_3)CN$, and of ion *m/z* 56 and 70 for the ^{14}N residue. In (B), M–X indicates that the molecular ion lost one X chemical group (see text for fragments labelling). The shift of the various fragments due to ^{15}N is observed and noted by *.

Table 1. Infrared band positions (cm^{-1}) and attributions for residues obtained from H_2O:HCN:CH_3CHO 1:0.5:0.7 ice mixtures at 210 K (Fig. 2B), H_2O:NH_3:CH_3CHO 1:0.9:0.5 at 200 and 250 K (Fig. 6B) and H_2O:NH_3:HCN:CH_3CHO 1:0.6:0.7:0.7 at 220 K (Fig. 8e). Infrared band positions of $_2$HNCH(CH_3)OH and HO–CH(CH_3)–CN are also reported as references. The band positions correspond to the product after water desorption.

Product expected IR bands (cm^{-1})			Residues IR bands (cm^{-1})				Theoretical IR bands (cm^{-1})
$_2$HN–CH(CH_3)OH	HO–CH(CH_3)–CN	Attributions	H_2O:HCN:CH_3CHO 1:0.5:0.7 (210 K)	H_2O:NH_3:CH_3CHO 1:0.9:0.5 200 K	H_2O:NH_3:CH_3CHO 1:0.9:0.5 250 K	H_2O:NH_3:HCN:CH_3CHO 1:0.6:0.7:0.7 (220 K)	H[OCH(CH_3)]$_n$–CN $n = 1$–3
3333	–	ν_{NH}	–	3326	–	–	–
–	3331	ν_{OH}	3350	–	–	–	3400–3100
3279	–	ν_{OH}	–	3256	3288	3292	–
–	2990	ν_{CHas}	2990	–	–	2988	2992
2973	–	ν_{CHas}	–	2971	2970	2973	–
	2940	ν_{CHs}	2940	–	–	2933	2940
2925	–	ν_{CHs}	–	2923	2910	2918	–
–	2250	ν_{CN}	2250	–	–	2247	2279
	–	δ_{NH}	–	1663	–	1666	–
1610	–	δ_{NH}	–	1600	–	1607	–
–	–	δ_{OH}	–	1490	1495	1498	–
–	–	δ_{OH}	–	–	–	1476	–
–	–		–	–	1455	1454	–
1446	1443	δ_{OH}	1444	1440	1433	–	1434
–	1409	δ_{OH}	–	–	–	–	1405
–	–		–	1400	–	–	–
–	–		1393	–	–	–	–
1372	1375	δ_{CH}	1377	1371	1371	1375	1370
–	–	δ_{CH}	–	–	1354	1356	–
–	–	δ_{CH}	–	–	1345	1349	–
–	–	δ_{CH}	–	1334	–	1331	–
–	1324	δ_{CH}	1329	–	1326	–	1312
–	–	δ_{CH}	1305	1309	1304	1306	–
–	1281	δ_{OHCH}	–	–	–	–	1275
1237	–		–	1236	–	–	–
–	–	$\nu_{C–O–Cas}$	–	1189	1178	1183	–
–	–	$\nu_{C–O–Cas}$	1162	–	–	1161	–
1136	–		–	1130	1131	1136	–
–	1111	$\nu_{C–O–C}$	1115	–	1109	1113	1101
1094	1095	$\nu_{C–O}$	1094	1081	1091	1096	1078
–	–	$\nu_{C–O}$	–	–	1076	1077	–
–	1047	$\nu_{C–C}$	1053	–	1057	1060	1042
–	–	$\nu_{C–Cs}$	–	973	975	977	–
–	–	$\nu_{C–Cs}$	962	–	–	961	–
916	–	$\nu_{C–N}$	–	–	–	–	–
–	–		900	–	–	896	–
–	–	$\nu_{C–N}$	–	865	871	873	–

The comparison of the residue and the standard with a theoretical calculation of a spectrum of a cluster of HO–(CH(CH_3))$_n$–CN polymers confirms the presence of polymers in the residue. First of all, the relative intensities of OH/CH_3 in the residue present a same trend. Furthermore, band number and their positions in the range 1500 to 750 cm^{-1} are highly similar between the residue and the theoretical calculation, especially for the bands at 963 cm^{-1} that is only present in the residue. Based on the theoretical spectrum, band attributions in the residue are displayed in Table 1. The mass spectrum of the residue was also compared with the mass spectrum of the standard (Fig. 4B). Ions at M^+–H, M^+–CH_3, M^+–OH and HCO^+ are observed in both cases. Although the relative intensities are not exactly the same, this comparison clearly indicates that our residue comprises H–(O–CH(CH_3))$_n$–CN compounds. With our mass spectrometer sensitivity, no masses are detected above *m*/*z* 75.

The TPD profiles of both the residue and the standard are obtained by monitoring the *m*/*z* 56 and/or 70 ions (Fig. 4C). The TPDs of the *m*/*z* 56 and 70 ions in the residue present a perfect correlation, showing that both ions come from the same compound. The TPD of the HOCH(CH_3)CN standard presents one desorption profile that can be fitted with a zero-order exponential, conveying a desorption energy of 55.5 ± 0.2 kJ mol^{-1} (6.7×10^3 K) ($\nu_0 = 10^{13}$ s^{-1}). The TPD of the residue presents two different profiles. One profile has a curvature similar to that of the standard when normalized to the second peak of the residue, which presents a similar desorption energy (55.8 ± 0.1 kJ mol^{-1} (6.7×10^3 K); $\nu_0 = 10^{13}$ s^{-1}, calculated from the fit of this profile). This suggests that the first compound desorbing from the residue is the HOCH(CH_3)CN monomer. The second profile gives a desorption energy of 57.7 ± 0.3 kJ mol^{-1} (6.9×10^3 K) ($\nu_0 = 10^{13}$ s^{-1}), which can correspond to HO–(CH(CH_3))$_n$–CN polymers, as the previous infrared and mass spectrometry results suggest. It has to be noted that the second peak is larger than the monomer peak, suggesting that a polymer distribution may be present.

3.2 Reactivity of an H_2O:HCN:NH_3:CH_3CHO ice mixture

Even if water is the most abundant molecule in the solid-phase of interstellar and cometary icy grains, other molecules are also present. Among them, NH_3 plays a central role due to its relative abundance and its active chemistry. The reactivity between NH_3 and aldehydes/ketones is well known and has been studied from

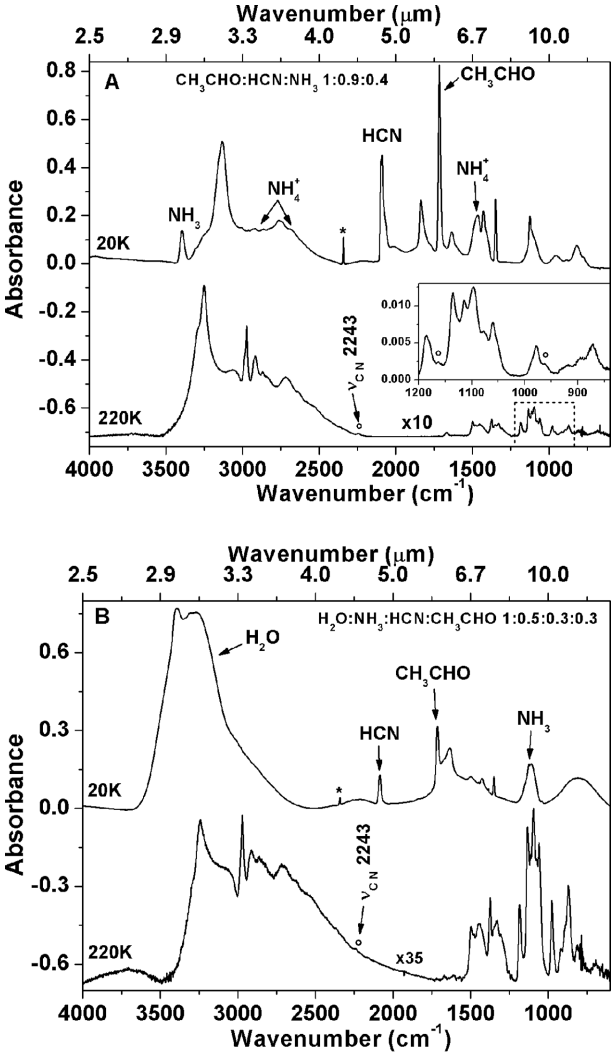

Figure 5. Infrared spectra of a CH_3CHO:HCN:NH_3 mixture in a 1:0.9:0.4 ratio (A) and of a H_2O:NH_3:HCN:CH_3CHO mixture in a 1:0.5:0.3:0.3 ratio (B) deposited at 20 K and measured at 220 K (50 min later after the standard warming procedure). The band marked with ∗ corresponds to CO_2 contamination and the ones marked with ○ refer to HO–CH(CH_3)–CN polymers.

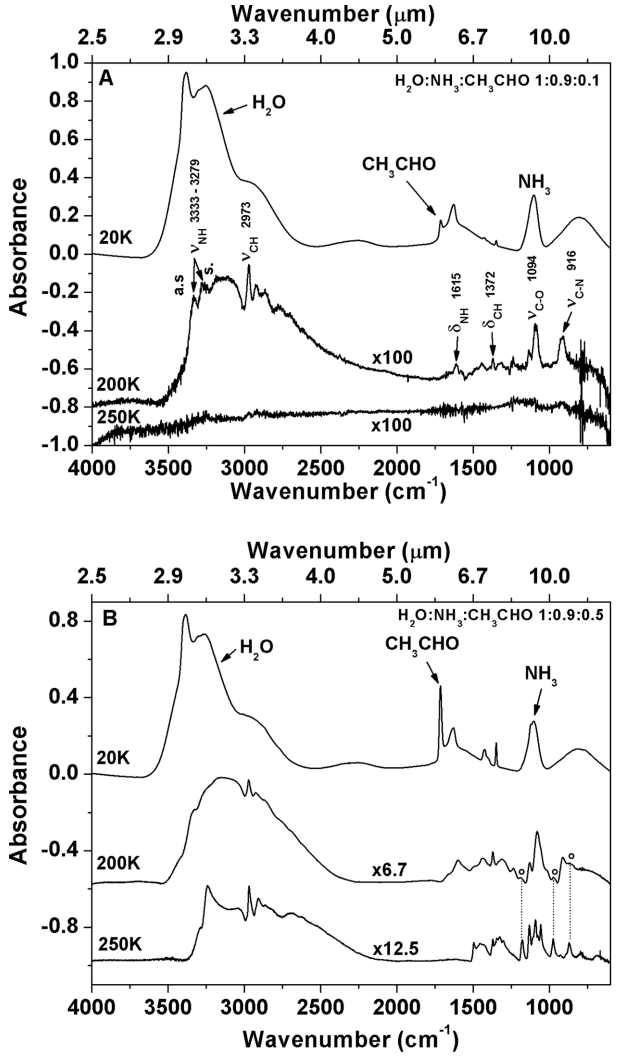

Figure 6. Infrared spectra of an H_2O:NH_3:CH_3CHO mixture deposited in a 1:0.9:0.1 ratio (A) and of an H_2O:NH_3:CH_3CHO mixture deposited in a 1:0.9:0.5 ratio at 20 K and measured at 200 K and finally at 250 K. The features displayed on the spectrum at 200 K in (A) are attributed to α-aminoethanol. In (B) the bands marked with ○ correspond to $_2$HN–($CH(CH_3)$–O)$_n$–H polymers.

laboratory analogue viewpoints (Bossa et al. 2009; Duvernay et al. 2010), concluding that aminoalcohols $NH_2C(R_1)(R_2)OH$ form. In the case of CH_3CHO, the condensation of ammonia leads to the formation of α-aminoethanol $NH_2CH(CH_3)OH$. Reactivity of CH_2O in the presence of NH_3 and HCN has been investigated and has shown a competition between the formation of aminomethanol and hydroxyacetonitrile (Danger et al. 2012). In this section, the reactivity between CH_3CHO and NH_3/HCN is studied in the presence and absence of H_2O.

A dry ice was formed at 20 K with CH_3CHO:HCN:NH_3 in a 1:0.9:0.4 ratio (Fig. 5A, up). At 20 K, different bands of the reactants are already observed. The band at 1471 cm^{-1} and the broadband at 2757 cm^{-1} correspond to the [NH_4^+ $^-$CN] salt, which is probably formed during deposition (Noble et al. 2013). Therefore, at 20 K, this ice is a mixture of CH_3CHO:HCN:NH_3:[NH_4^+ $^-$CN]. It was then warmed up at a temperature ramp of 4 K min^{-1}. After desorption of the initial compounds, numerous bands are present (shown in Fig. 5A, down). In the infrared spectrum of the residue at 220 K, two bands at 1163 and 961 cm^{-1} (inset image of Fig. 5A) and a nitrile band at 2243 cm^{-1} can be attributed to HOCH(CH_3)CN. Numerous other bands are also present (refer to Table 1), but some do not match with the HOCH(CH_3)CN compound. Under the conditions described here, the only other reaction that can occur is NH_3 with CH_3CHO, which in water diluted conditions should lead to the formation of $_2$HN–CH(CH_3)–OH. However, this product desorbs at a temperature lower than 220 K (Duvernay et al. 2010).

Moreover, knowing that the reactivity between NH_3 and CH_2O also leads to the formation of $_2$HN–(CH_2–O)$_n$–H polymers depending on the dilution conditions (Danger et al. 2012), we suggest that these features may fit with those of $_2$HN–($CH(CH_3)$–O)$_n$–H polymers. Remarkably, very similar trends are obtained when H_2O is present in the initial ice composition (Fig. 5B).

In order to confirm these assumptions, the same experiments were performed with ices without HCN and with various amounts of CH_3CHO (Figs 6A and B). For low CH_3CHO concentrations, $_2$HN–CH(CH_3)–OH is detected at 200 K (Fig. 6A) and after its desorption, no products are observed in the infrared spectrum at

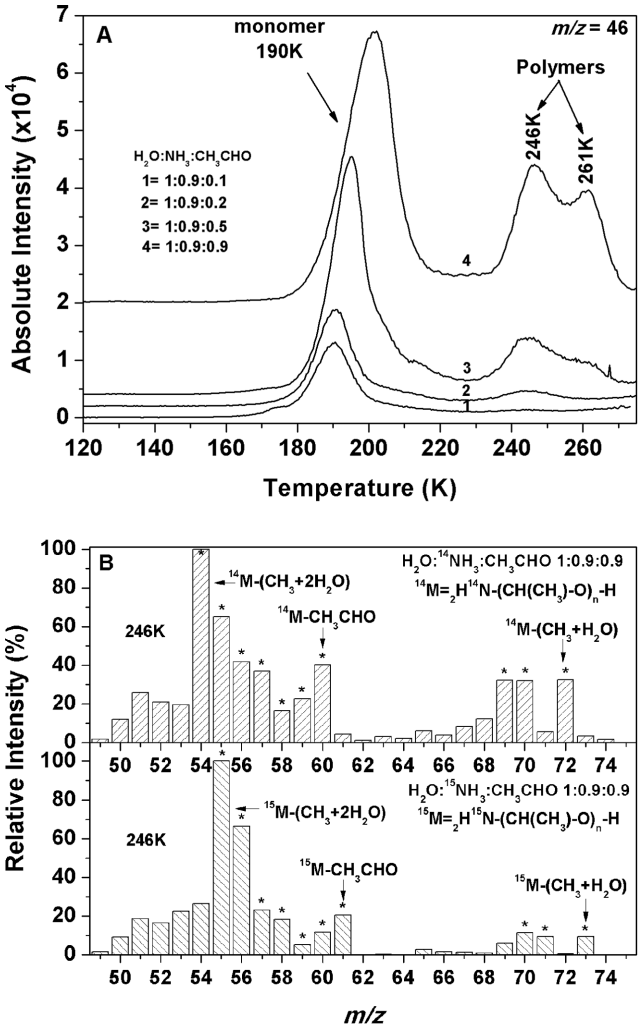

Figure 7. Profile of the ion *m*/*z* 46 as a function of temperature for compounds desorbing during the warming of ices containing H_2O, NH_3 and CH_3CHO at 20 K. H_2O:NH_3:CH_3CHO comprise these ices in the following ratios: (1) 1:0.9:0.1, (2) 1:0.9:0.2, (3) 1:0.9:0.5 and (4) 1:0.9:0.9 (A). The mass spectra of residue desorbing at 246 K of ice in a 1:0.9:0.9 ratio are displayed in (B) for an ice containing $^{14}NH_3$ (top) or $^{15}NH_3$ (bottom). Fragments including N are indicated by ∗ on spectra for both isotopologues. M–X indicates that the molecular ion lost one X chemical group (see text for fragments labelling).

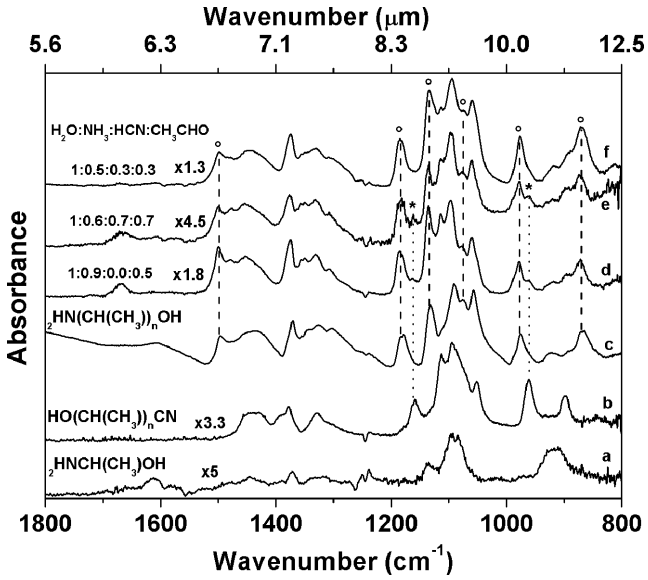

Figure 8. Comparison of infrared spectra in the 800—1800 cm^{-1} range at 200 K for α-aminoethanol (a: Fig. 6A), at 210 K for the hydroxypropionitrile polymers (b: Fig. 2B), at 220 K for polymers of α-aminoethanol (c: Fig. 6B), at 220 K for hydroxypropionitrile and α-aminoethanol polymers without ice water (d: Fig. 5A), at 220 K for hydroxypropionitrile and α-aminoethanol polymers obtained from a concentrated ice (e), and at 230 K for hydroxypropionitrile and α-aminoethanol polymers obtained from a diluted ice (f: Fig. 5B). The bands marked with ○ correspond to $_2$HN–(CH(CH_3)–O)$_n$–H polymers, while the ones marked with ∗ correspond to HO–(CH(CH_3))$_n$–CN polymers. For readability, a different factor has been applied to each IR spectrum.

250 K. In contrast, for larger CH_3CHO concentrations (Fig. 6B), the most characteristic bands of $_2$HN–CH(CH_3)–OH are also present at 200 K, but are disappearing at 250 K. However, other bands that were observed at 200 K (1184, 970 and 865 cm^{-1}) still remain at 250 K. Similar to results for the reaction between CH_2O and NH_3, these infrared features can be attributed to polymers of $_2$HN–(CH(CH_3)–O)$_n$–H.

Mass spectra were also monitored during the desorption of these residues. Fig. 7(A) displays TPD of *m*/*z* 46 of $_2$HN–(CH(CH_3)–O)$_n$–H monomer and polymers, which is the most characteristic ion of these compounds, since it is present both in the monomer and polymers. When the CH_3CHO is highly diluted in the initial ice (Fig. 7A, 1), only ions coming from $_2$HN–CH(CH_3)–OH are observed at 190 K. In contrast, for larger initial concentrations of CH_3CHO (Fig. 7A, 2–4), in addition of contribution from $_2$HN–CH(CH_3)–OH, other contributions appear at 246 K and at 261 K, which moreover increase in positive correlation with the CH_3CHO initial abundance. A comparison between the mass spectra of the residue formed from $^{14}NH_3$ and $^{15}NH_3$ (Fig. 7B) shows that these compounds have N-bearing chemical functionalities, since an *m*/*z* shift of +1 is observed between these two residues.

Furthermore, their mass spectra present larger *m*/*z* ions than the *m*/*z* peak associated with the mass of the monomer, confirming the presence of $_2$HN–(CH(CH_3)–O)$_n$–H polymers, as previously suggested. Consequently, the ratio between α-aminoethanol with respect to its polymers depends on the initial abundance of CH_3CHO in the ice: the larger the initial amount of CH_3CHO, the larger the probability of polymer formation (Fig. 7B relative to the highest CH_3CHO abundance).

Fig. 8 displays a comparison of the infrared spectra in the 1800–800 cm^{-1} range between the residues formed in the presence of H_2O: $_2$HN–CH(CH_3)–OH (a, 200 K), H–(O–CH(CH_3)–)$_n$–CN (b, 210 K), $_2$HN–(CH(CH_3)–O)$_n$–H (c, 220 K), the residue formed without H_2O (d, 220 K) and the residues formed in the presence of H_2O with various amounts of HCN and CH_3CHO (e and f, 220 K). The $_2$HN–CH(CH_3)–OH compound is not present in the residues or as a trace (see Table 1) because it fully sublimes at temperatures higher than 200 K. However, at least six characteristic bands of its polymers are present at 870, 976, 1075, 1135, 1182 and 1498 cm^{-1}. In addition to these polymers, in the residue formed without H_2O (d), two other bands can be attributed to the H–(O–CH(CH_3))$_n$–CN polymers at 961 and 1163 cm^{-1}. Furthermore, the stretching mode of CN is also present at 2243 cm^{-1}, confirming their presence. In the presence of H_2O, the same bands are observed for the concentrated CH_3CHO ice (e), whereas for the diluted ice (f) bands related to the $_2$HN–(CH(CH_3)–O)$_n$–H polymers are

observed only. H–(O–CH(CH_3))$_n$–CN polymers present relatively low intensities: the 1131 cm^{-1} band is unobservable while the one at 961 cm^{-1} can be identified in the shoulder of a band related to the $_2$HN–(CH(CH_3)–O)$_n$–H polymers. Furthermore, as described in Fig. 5(B), the presence of H–(O–CH(CH_3))$_n$–CN polymers is confirmed by a ν_{CN} band at 2243 cm^{-1}.

These results show that from an initial ice containing H_2O:NH_3:HCN:CH_3CHO a competition between the formation of α-aminoethanol polymers and hydroxypropionitrile polymers takes place. Larger initial concentrations of NH_3 drive the reaction to formation of α-aminoethanol and its related polymers.

3.3 Quantum chemical simulations of the reactions

In order to have deeper insights into the formation of HOCH(CH_3)CN and $_2$HN–CH(CH_3)–OH in the experimental conditions, we elucidated the mechanistic steps of these processes by calculating their PESs at a quantum chemical level. These calculations were based on a cluster model approach, in which the initial ices were represented by different compositions depending on the reaction to study. Experimentally, we found that HOCH(CH_3)CN forms from ices with composition of CH_3CHO:HCN:H_2O, CH_3CHO:HCN:NH_3 and CH_3CHO:HCN:NH_3:H_2O. Here we calculated the formation of HOCH(CH_3)CN considering these three situations. Fig. 9 shows the structures involved in the formation of HOCH(CH_3)CN from an initial ice matrix of CH_3CHO:HCN:H_2O. For this particular case, the cluster model of the reactant consisted of one CH_3CHO molecule and four HCN molecules embedded in a 12-water molecules matrix (see Fig. 9a, REACT_1).

Figs 9(B) and (C) show the calculated PES of the formation of HOCH(CH_3)CN adopting this ice cluster model. The first step is a proton transfer from HCN to the adjacent water molecule, in which an H_3O^+/CN^- ion pair forms (INT0_1). This intermediate formation is followed by the coupling of the CN moiety to the carbonyl C atom of CH_3CHO (TS1_1) to form the negatively charged $^-$OCH(CH_3)CN intermediate species (see INT1_1). The INT_1 structure is still an ion pair, in which the $^-$OCH(CH_3)CN coexists with the hydronium H_3O^+ ion. Interestingly, both INT0_1 and INT1_1 are only possible if the positive and negative charges of the ion pair partners are stabilized by hydrogen bond interactions as those established with the surrounding H_2O molecules. Finally, a proton transfer from the H_3O^+ to the $^-$OCH(CH_3)CN (TS2_1) leads to the formation of the final HOCH(CH_3)CN product (PROD). Table 2 reports the calculated relative free energies (with respect to REACT_1) at 20 and 220 K and the calculated rate constants using the classical Eyring equation and the corresponding half-life times ($t_{1/2}$); namely the time necessary to consume the half amount of reactant. The highest energy barrier step is the second one which corresponds to the attack of CN^- on CH_3CHO. At 20 K, the reaction does not evolve, as indicated by this calculated rate constant, but it is surmountable at 220 K with an estimated $t_{1/2}$ of about 1 min.

Formation of HOCH(CH_3)CN by reaction of CH_3CHO with HCN was also observed in the presence of NH_3 and NH_3/H_2O ices. In both cases, during the ice matrix deposition, the [NH_4^+ $^-$CN] salt was formed. Fig. 10 shows the PESs of the formation of this salt through a proton transfer from HCN to NH_3. Fig. 10(A) in the presence of only NH_3 with a cluster model made up by 1 CH_3CHO molecule and 4 HCN and 12 NH_3 molecules, and Fig. 10(B) in the presence of an NH_3/H_2O ice matrix modelled by a cluster consisting of 1 CH_3CHO molecule and 3 HCN, 3 NH_3 and 10 H_2O molecules. For both cases, the calculated PESs present very low energy barriers. The very same low values are obtained in terms of

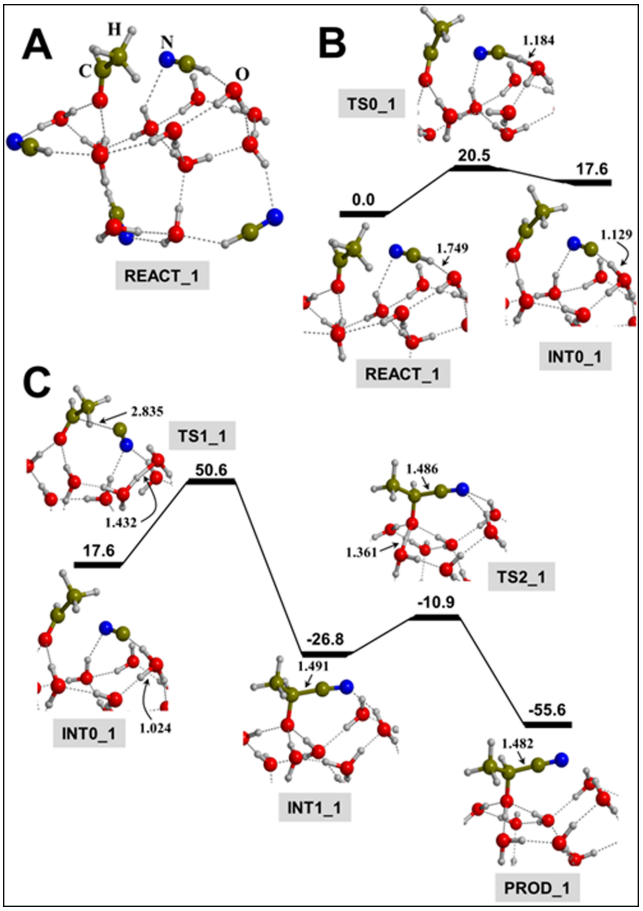

Figure 9. (A) B3LYP-D3/6–311++G(d,p) optimized structure of the cluster model used for the formation of HOCH(CH_3)CN from an ice mixture with a CH_3CHO:HCN:H_2O composition. (B) B3LYP-D3/6–311++G(d,p) energy profile including the zero-point energy (ZPE) corrections (in kJ mol^{-1}) for the formation of HOCH(CH_3)CN using the cluster model shown in (A). Only the most chemically active part is shown, for the sake of clarity. The zero-energy reference is REACT_1. Bond lengths are in Å. All free values have been calculated at 0 K.

relative free energies at 20 K (see Table 2), whose calculated k and $t_{1/2}$ indicate that the formation of this salt is very fast. It is worth mentioning that the very same first process (namely, proton transfer from HCN to the ice matrix) also takes place in the formation of HOCH(CH_3)CN with only H_2O ice (see Fig. 9B). However, the energies of this step are calculated to be unfavourable at 20 K and accordingly, formation of the [H_3O^+ $^-$CN] salt is not observed in the experiments. Fig. 11 presents the calculated PESs related to the formation of HOCH(CH_3)CN in the presence of NH_3 (A) and NH_3/H_2O (B) ices starting from the already formed NH_4^+/CN^- ion pair. For both systems, the calculated paths adopt the same two-step mechanism: (i) C–C coupling between CN^- and CH_3CHO to form the INT4 $^-$OCH(CH_3)CN anion, and (ii) proton transfer from the NH_4^+ to the negatively charged oxygen atom of $^-$OCH(CH_3)CN to form HOCH(CH_3)CN. This last step, however, is direct in the presence of only NH_3, whereas it is assisted by H_2O with NH_3/H_2O. This difference is due to the fact that the NH_4^+ cation is strongly stabilized by H-bond interactions with water molecules, whereas this is not the case with NH_3, which causes the motion of NH_4^+ to directly interact with $^-$OCH(CH_3)CN.

These structural differences are probably the reason because the overall energy with only NH_3 is lower than with NH_3/H_2O.

Table 2. B3LYP-D3/6–311++G(d, p) relative free energies (ΔG_{rel}, in kJ mol^{-1} or kK) computed at 20 and 220 K of the stationary points for the formation of HO–CH(CH_3)–CN and $_2$HN–CH(CH_3)–OH. Calculated rate constants (in s^{-1}) and half-life times ($t_{1/2}$, in s) for the corresponding free energy barriers at these temperatures are also included. These values were obtained using a $\nu_o = 10^{13}$ s^{-1}.

Ice mixture	Structure	$T = 20$ K			$T = 220$ K			Product
		ΔG_{rel} (kJ mol^{-1}/kK)	k [a] (s^{-1})	$t_{1/2}$ (s)	ΔG_{rel} (kJ mol^{-1}/kK)	k [a] (s^{-1})	$t_{1/2}$ (s)	
CH_3CHO/HCN/H_2O Fig. 9	**REACT_1**	0.0/**0.0**			0.0/**0.0**			**HOCH(CH_3)CN**
	TS0_1	21.8/**2.6**	6.2×10^{-46}	1.1×10^{45}	28.5/**3.4**	8.1×10^{5}	8.6×10^{-7}	
	INT0_1	15.9/**1.9**			20.5/**2.5**			
	TS1_1	52.3/**6.3**	1.1×10^{-125}	6.6×10^{124}	61.9/**7.4**	9.1×10^{-3}	7.6×10^{1}	
	INT1_1	−15.1/−**6.9**			15.1/**1.8**			
	TS2_1	0.8/**0.1**	1.2×10^{-30}	5.6×10^{29}	31.0/**3.7**	2.0×10^{5}	3.4×10^{-6}	
	PROD_1	−37.2/−**4.5**			−6.7/−**0.8**			
NH_3/HCN Fig. 10(A)	**REACT_2**	0.0/**0.0**			0.0/**0.0**			**[NH_4^+−CN]**
	TS_2	1.7/**0.2**	1.8×10^{7}	3.9×10^{-8}	5.0/**0.6**	2.9×10^{11}	2.4×10^{-12}	
	PROD_2	−7.1/−**0.8**			−1.7/−**0.2**			
NH_3/HCN/H_2O Fig. 10(B)	**REACT_3**	0.0/**0.0**			0.0/**0.0**			
	TS_3	0.8/**0.1**	2.7×10^{9}	2.5×10^{-10}	4.6/**0.5**	3.7×10^{11}	1.9×10^{-12}	
	PROD_3	−14.2/−**1.7**			−7.1/−**0.8**			
CH_3CHO/HCN/NH_3 Fig. 11(A)	**PROD_2**	0.0/**0.0**			0.0/**0.0**			**HOCH(CH_3)CN**
	TS1_4	42.3/**5.0**	1.8×10^{-99}	3.9×10^{98}	60.7/**7.3**	1.8×10^{-2}	3.8×10^{1}	
	INT_4	−32.6/−**3.9**			−9.2/−**1.1**			
	TS2_4	−28.0/−**3.4**	4.0×10^{-1}	1.7	2.9/**0.3**	6.0×10^{9}	1.1×10^{-10}	
	PROD_4	−44.8/−**5.4**			−25.9/−**3.1**			
CH_3CHO/HCN/NH_3/H_2O Fig. 11(B)	**PROD_3**	0.0/**0.0**			0.0/**0.0**			
	TS1_5	53.1/**6.4**	6.9×10^{-128}	1.0×10^{127}	67.4/**8.1**	4.6×10^{-4}	1.5×10^{3}	
	INT_5	−13.4/−**1.6**			4.6/**0.5**			
	TS2_5	10.0/**1.2**	2.7×10^{-50}	2.6×10^{49}	32.2/**3.9**	1.0×10^{5}	6.7×10^{-6}	
	PROD_5	−43.1/−**5.2**			−23.8/−**2.9**			
CH_3CHO/HCN/NH_3 Fig. 12(B)	**REACT_6**	0.0/**0.0**			0.0/**0.0**			**$_2$HNCH(CH_3)OH**
	TS1_6	46.0/**5.5**	2.6×10^{-109}	2.7×10^{108}	49.8/**6.0**	6.9	1.0×10^{-1}	
	INT_6	20.5/**2.5**			25.1/**3.0**			
	TS2_6	27.2/**3.3**	3.9×10^{-60}	1.8×10^{59}	30.5/**3.7**	2.6×10^{5}	2.7×10^{-6}	
	PROD_6	−7.9/−**0.1**			−4.6/−**0.5**			
CH_3CHO/HCN/NH_3/H_2O Fig. 13(B)	**REACT_7**	0.0/**0.0**			0.0/**0.0**			
	TS1_7	27.6/**3.3**	3.1×10^{-61}	2.2×10^{60}	19.2/**2.3**	1.2×10^{8}	5.6×10^{-9}	
	INT_7	12.6/**1.5**			12.1/**1.4**			
	TS2_7	29.3/**3.5**	1.3×10^{-65}	5.2×10^{64}	33.5/**4.0**	5.2×10^{4}	1.3×10^{-5}	
	PROD_7	−10.5/−**1.3**			−7.1/−**0.8**			

Notes. [a]Rate constants were calculated considering the intrinsic energy barriers, that is, the free energy difference between the transition state and the minimum structure (reactant or intermediate) of lowest energy.

Irrespective of these differences, calculation of k and $t_{1/2}$ derived from the calculated free energy barriers (Table 2) indicates that formation of HOCH(CH_3)CN is only possible at 220 K, contrarily to 20 K.

In addition to formation of HOCH(CH_3)CN, we found that $_2$HN–CH(CH_3)–OH can also form in our experimental conditions. Formation of this compound occurs both with NH_3/HCN and with NH_3/HCN/H_2O ice mixtures. The cluster models used to simulate the formation of $_2$HN–CH(CH_3)–OH have the same composition as those employed for the formation of HO–CH(CH_3)CN but differ in the molecule spatial distribution; i.e. the reacting HCN and NH_3 molecules were exchanged in their respective positions. The initial structures are shown in Figs 12(A) and 13(A) for the processes with NH_3/HCN and NH_3/HCN/H_2O, respectively. The calculated PES with NH_3/HCN is shown in Fig. 12(B).

The first step involves an N–C coupling between the reacting NH_3 molecule and CH_3CHO, which is followed by a proton transfer from the reacting NH_3 to an adjacent NH_3, which is converted into a NH_4^+ cation, leading to the INT6 $_2$HN–CH(CH_3)–O^- anion. The second step is a proton transfer from NH_4^+ to $_2$HN–CH(CH_3)–O^- forming the $_2$HN–CH(CH_3)–OH final compound. The reaction mechanism is quite similar with NH_3/HCN/H_2O, whose PES is shown in Fig. 13(B). The first step is also an N–C coupling between the reactants. However, at variance with NH_3/HCN, the intermediate species that is formed is the INT7 $^+{}_3$HN–CH(CH_3)–O^- zwitterion, which is stabilized by the hydrogen bonds established with the H_2O molecules. Formation of $_2$HN–CH(CH_3)–OH is achieved by proton transfer from the –NH_3^+ moiety to the negatively charged O atom, which is assisted by the H_2O ice matrix molecules. The calculated free energy barriers and the corresponding k and $t_{1/2}$ values (Table 2) for both processes, indicate that at 20 K formation of $_2$HN–CH(CH_3)–OH is kinetically hampered, whereas at 220 K the reactions can proceed.

To sum up, the limiting step in these reactions is the nucleophilic attack of CN^- or NH_3 on CH_3CHO except if H_2O is present since H_2O catalyses the condensation of NH_3 on CH_3CHO. In this latter

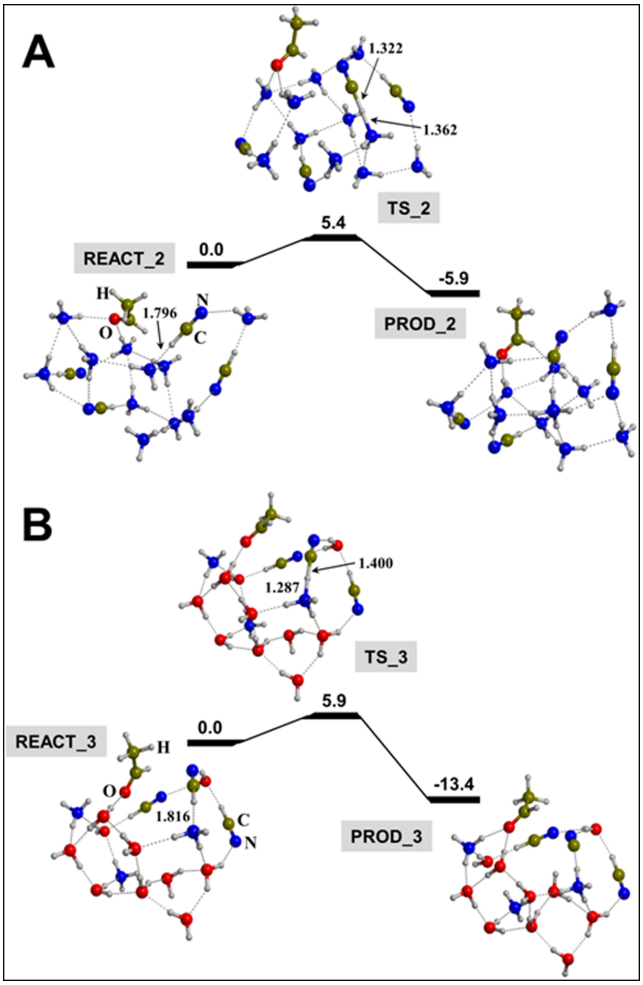

Figure 10. B3LYP-D3/6–311++G(d,p) energy profile including the zero-point energy (ZPE) corrections (in kJ mol^{-1}) for the formation of the NH_4^+/CN^- ion pair from an ice mixture of CH_3CHO:HCN:NH_3 (A) and CH_3CHO:HCN:NH_3:H_2O (B). The zero-energy reference is REACT_2 for panel (A) and REACT_3 for panel (B). Bond lengths are in Å. All free values have been calculated at 0 K.

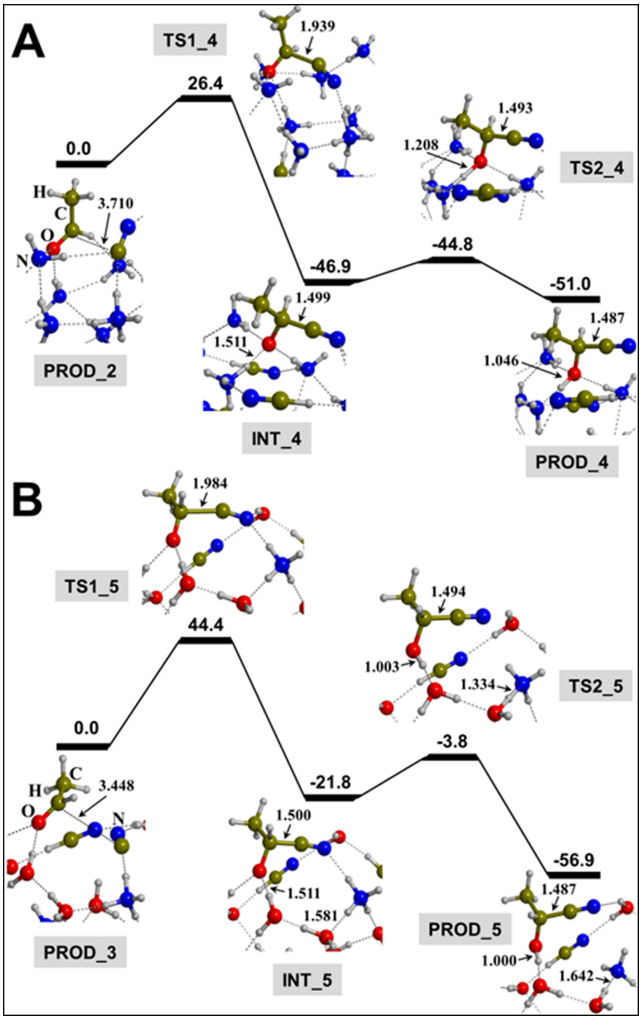

Figure 11. B3LYP-D3/6–311++G(d,p) energy profile including the zero-point energy (ZPE) corrections (in kJ mol^{-1}) for the formation of $HOCH(CH_3)CN$ from an ice mixture of CH_3CHO:HCN:NH_3 (A) and CH_3CHO:HCN:NH_3:H_2O (B) The zero-energy reference is PROD_2 for panel (A) and PROD_3 for panel (B), which are the NH_4^+/CN^- ion pair-containing species shown in Fig. 10. Only the most chemically active part is shown, for the sake of clarity. Bond lengths are in Å. All free values have been calculated at 0 K.

case, the limiting step is the proton transfer to obtain the neutral product. It has also to be noted that the reaction kinetic of NH_3 on CH_3CHO is twelve orders of magnitude faster than CN^- on CH_3CHO in the presence of H_2O and three orders of magnitude faster without H_2O. Consequently, from an equal amount of CN^- and NH_3 in the initial ice, CH_3CHO will be consumed faster by NH_3. The aminoalcool $_2HNCH(CH_3)_nOH$ is thus the preferred product. Interestingly, in our experiments, not only the $HOCH(CH_3)CN$ and $_2HN–CH(CH_3)–OH$ compounds were formed, but the related polymers were also detected. The calculated PESs exposed above are consistent with these findings. That is, all the calculated mechanisms predict the formation of transient negatively charged intermediates. These species, instead of being protonated, can react with other CH_3CHO molecules available in the ice mixture, in which the negatively O atom can be attached to the C atom of the new CH_3CHO molecule. This reaction elongates the backbone chain so it can be understood as the first step towards polymer formation. Accordingly, reaction of CH_3CHO with $^-OCH(CH_3)CN$ (INT4 or INT5) leads to the formation of $^-OCH(CH_3)–OCH(CH_3)CN$, whereas with $_2HN–CH(CH_3)–O^-$ (INT6) and the $^+{}_3HN–CH(CH_3)–O^-$ (INT7) to $_2HN–CH(CH_3)–O–CH(CH_3)–O^-$ and $^+{}_3HN–CH(CH_3)–O–CH(CH_3)–O^-$, respectively. This elongation can further be continued by reaction with other CH_3CHO molecules and the polymerization can be truncated by protonating the negatively O end, thus leading to the final neutral polymer. Formation of the HO–CH_2–O–CH_2–CN dimer was already computed by some of us by reaction of two CH_2O molecules with HCN in the presence of an H_2O-dominated ice (Danger et al. 2014).

4 THERMAL REACTIVITY OF ACETALDEHYDE IN ASTROPHYSICAL ICES

From the results presented here, as well as those described in Duvernay et al. 2010), we can draw a general scheme of the CH_3CHO reactivity in astrophysical ices containing H_2O, NH_3 and/or HCN (sketched in Fig. 14). When an ice mixture consisting of CH_3CHO and HCN is progressively warmed, no reactivity occurs because HCN is not reactive; i.e. it must be dissociated beforehand. HCN can be activated by H_2O or NH_3. H_2O assists the

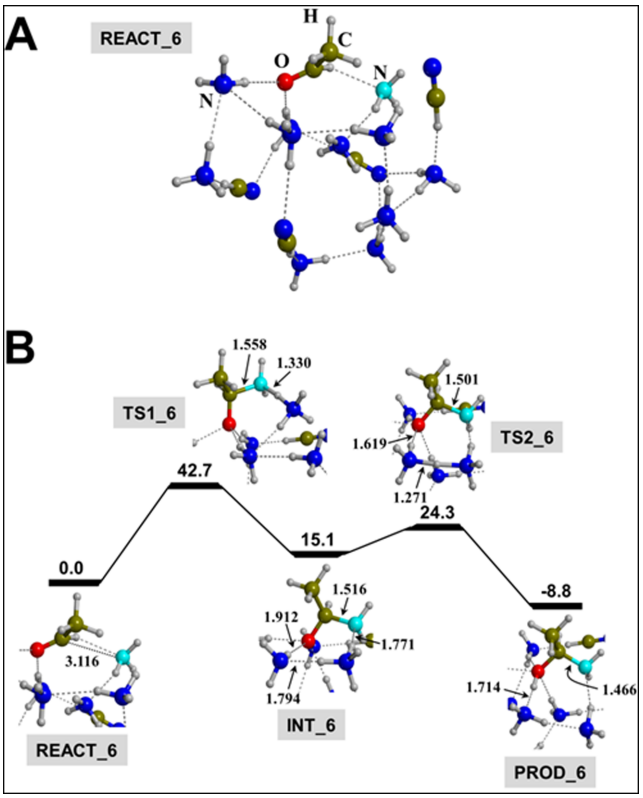

Figure 12. (A) B3LYP-D3/6–311++G(d,p) optimized structure of the cluster model used for the formation of $_2$HN–CH(CH$_3$)–OH from an ice mixture with a CH$_3$CHO:HCN:NH$_3$ composition. (B) B3LYP-D3/6–311++G(d,p) energy profile including the zero-point energy (ZPE) corrections (in kJ mol^{-1}) for the formation of $_2$HN–CH(CH$_3$)–OH using the cluster model shown in (A). Only the most chemically active part is shown, for the sake of clarity. The zero-energy reference is REACT_6. Bond lengths are in Å. All free values have been calculated at 0 K.

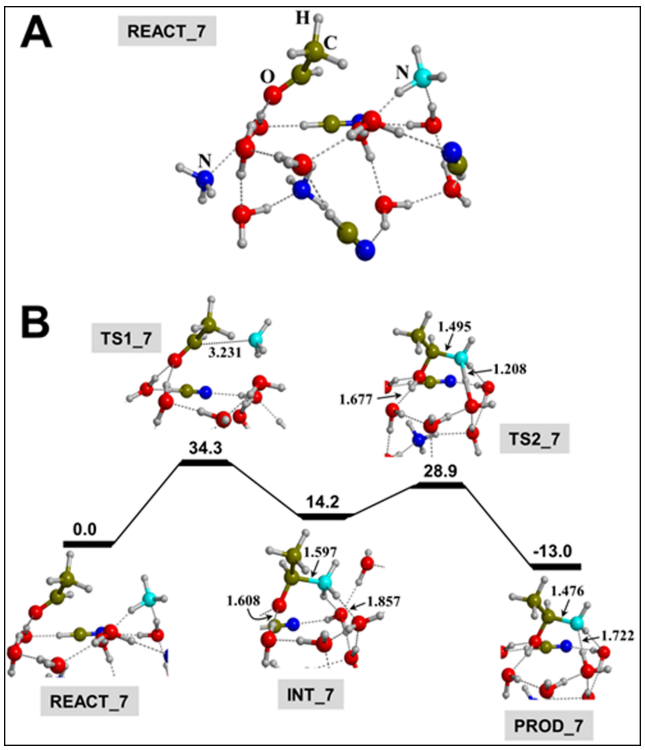

Figure 13. (A) B3LYP-D3/6–311++G(d,p) optimized structure of the cluster model used for the formation of $_2$HN–CH(CH$_3$)–OH from an ice mixture with a CH$_3$CHO:HCN:NH$_3$:H$_2$O composition. (B) B3LYP-D3/6–311++G(d,p) energy profile including the zero-point energy (ZPE) corrections (in kJ mol^{-1}) for the formation of $_2$HN–CH(CH$_3$)–OH using the cluster model shown in (A). Only the most chemically active part is shown, for the sake of clarity. The zero-energy reference is REACT_7. Bond lengths are in Å. All free values have been calculated at 0 K.

dissociation of HCN, yielding a transient CN$^-$ ion that immediately reacts with acetaldehyde (the free energy barrier at 220 K, $\Delta G^{\neq}_{220}$, is 28.5 kJ mol^{-1}/3.4 kK, see TS0_1 of Table 2). The resulting products are the 2-hydroxypropionitrile (HO–CH(CH$_3$)–CN) and its related polymers (H–(O–CH(CH$_3$))$_n$–CN) (for HO–CH(CH$_3$)–CN, $\Delta G^{\neq}_{220} = 61.9$ kJ mol^{-1}/7.4 kK, see TS1_1 of Table 2). NH$_3$ also activates the HCN dissociation, but in a different way. NH$_3$ reacts with HCN at low temperature forming the [NH$_4^+$ $^-$CN] salt ($\Delta G^{\neq}_{220}$ = 5.0 kJ mol^{-1}/0.6 kK, see TS_2 of Table 2). In this case, CN$^-$ is a stable anion that can react with CH$_3$CHO, also leading to H–(O–CH(CH$_3$))$_n$–CN ($\Delta G^{\neq}_{220} = 60.7$ kJ mol^{-1}/7.3 kK, see TS1_4 of Table 2). However, this reaction channel competes with the formation of α-aminoethanol ($_2$HN–CH(CH$_3$)–OH), since NH$_3$ can also directly react with CH$_3$CHO ($\Delta G^{\neq}_{220} = 49.8$ kJ mol^{-1}/6.0 kK, see TS1_6 of Table 2). Moreover, in the presence of H$_2$O, the reaction is catalysed ($\Delta G^{\neq}_{220} = 19.2$ kJ mol^{-1}/2.3 kK, see TS1_7 of Table 2).

Therefore, from an ice containing CH$_3$CHO:NH$_3$:HCN, irrespective of the presence of H$_2$O, both HO–CH(CH$_3$)–CN and $_2$HN–CH(CH$_3$)–OH can be formed. Large initial concentrations of CH$_3$CHO also lead to the formation of the related polymers H–(O–CH(CH$_3$))$_n$–CN and $_2$HN–(CH(CH$_3$)–O)$_n$–H. However, as already noted in Section 3.3, $_2$HN–CH(CH$_3$)–OH forms faster than HO–CH(CH$_3$)–CN ($\Delta G^{\neq}_{220} = 19.2$ kJ mol^{-1}/2.3 kK (TS1_7 of Table 2) and $\Delta G^{\neq}_{220}$ = 67.4 kJ mol^{-1}/8.1 kK (TS1_5 of Table 2), respectively) and it is thus the preferred product. Furthermore, if realistic

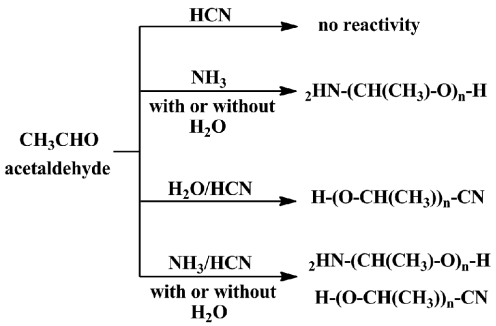

Figure 14. Reactivity of acetaldehyde CH$_3$CHO as observed in laboratory conditions simulating reactivity in astrophysical ices (high vacuum 10^{-9} mbar, solid phase 20–300 K) containing H$_2$O, NH$_3$ and/or HCN.

astrophysical ice compositions are used; i.e. concentrations of NH$_3$ higher than the HCN ones, a prevalence of $_2$HN–(CH(CH$_3$)–O)$_n$–H formation is also observed compared to H–(O–CH(CH$_3$))$_n$–CN, which is only present in trace amounts (see Fig. 5B). This is of great relevance in the astrochemical context because formation of $_2$HN–CH(CH$_3$)–OH is the first step towards alanine formation in the Strecker synthesis. Therefore, it seems that CH$_3$CHO and CH$_2$O react with both NH$_3$ and HCN, even if the reaction with CH$_3$CHO requires higher activation energy due to the increase of steric hindrance around the carbonyl. At variance with CH$_2$O, however, it is worth mentioning that reactions involving CH$_3$CHO yield the

formation of chiral compounds, so that chiral compounds can be formed in the bulk of icy grains in astrophysical environments if the local energy is sufficient. This has not been explored in detail in our experiments since only racemic mixtures are formed (i.e. no enantiomeric excess), but new experiments specifically devoted to investigate the enantiomeric synthesis of organic compounds in astrophysical ices will certainly contribute to the understanding of this fundamental aspect.

5 CONCLUSIONS

In this contribution, the reactivity of acetaldehyde (CH_3CHO) in astrophysical ice analogues was investigated in the presence of NH_3 and/or HCN, both in the presence and absence of H_2O, by using infrared and mass spectrometry measurements in combination with quantum chemical calculations. Pure ices consisting of CH_3CHO and HCN do not show reactivity during the warming. However, in the presence of H_2O, NH_3, or an NH_3/H_2O mixture, reaction occurs leading to the formation of 2-hydroxypropionitrile (HO–$CH(CH_3)$–CN). Moreover, in the presence of NH_3, a competing reaction leading to the formation of α-aminoethanol ($_2$HN–$CH(CH_3)$–OH) also takes place. Therefore, measurements based on infrared spectroscopy and mass spectrometry indicate that from an ice with an initial composition of H_2O:NH_3:HCN:CH_3CHO that is progressively warmed, two different products are formed: HO–$CH(CH_3)$–CN and $_2$HN–$CH(CH_3)$–OH. Characterization of their PESs at the B3LYP-D3 level supports these findings. The relative abundance of NH_3/HCN in the initial ice determines the final ratio between these two compounds. When this ratio increases, formation of $_2$HN–$CH(CH_3)$–OH becomes preponderant. Polymers of these two compounds also formed, whose amounts depend on the initial concentrations in the ice; the larger the CH_3CHO initial concentration, the more polymer formation. These results are of great relevance in elucidating those pathways that can contribute to the formation of amino acid precursors from reactions occurring in the bulk of astrophysical ices. In this work, it is shown that, by adopting realistic compositions of astrophysical ices (i.e. larger concentrations of NH_3 than HCN), formation of $_2$HN–$CH(CH_3)$–OH is uniquely more favourable compared to HO–$CH(CH_3)$–CN formation. This finding is of paramount importance because it points out that the first step of the Strecker synthesis involved in the formation of alanine ($_2$HN–$CH(CH_3)$–COOH), the simplest chiral amino acid, is an operating chemical channel.

ACKNOWLEDGEMENTS

This work has been funded by the French national program 'Physique Chimie du Milieu Interstellaire' (P.C.M.I, INSU), 'Environnements Planetaires et Origines de la Vie' (EPOV, CNRS), 'Programme National de Planétologie' (PNP, CNRS), the 'Centre National d'Etudes Spatiales' (C.N.E.S) from its exobiology program and PhD grant from Région Provence-Alpes-Côte d'Azur (PACA). This work was further supported by the ANR project VAHIIA (Grant ANR-12-JS08–0001–01) of the French Agence Nationale de la Recherche. AR is indebted to Programa Banco de Santander for a UAB distinguished postdoctoral research contract. Financial support from MICINN (projects CTQ2013–40347-ERC and CTQ2011–24847/BQU) and the use of the Catalonia Supercomputer Centre (CESCA) and of Barcelona Supercomputing Center through the QCM-2014–3–0032 project are gratefully acknowledged.

REFERENCES

Becke A. D., 1993, J. Chem. Phys., 98, 1372
Bernstein M. P., Sandford S. A., Allamandola L. J., 1997, AJ, 476, 932
Borget F., Danger G., Duvernay F., Chomat M., Vinogradoff V., Theulé P., Chiavassa T., 2012, A&A, 541, A114
Bossa J. B., Theulé P., Duvernay F., Chiavassa T., 2009, AJ, 707, 1524
Burton A. S., Stern J. C., Elsila J. E., Glavin D. P., Dworkin J. P., 2012, Chem. Soc. Rev., 41, 5459
Danger G., Borget F., Chomat M., Duvernay F., Theulé P., Guillemin J.-C., Le Sergeant D'Hendecourt L., Chiavassa T., 2011, A&A, 535, A47
Danger G., Duvernay F., Theulé P., Borget F., Chiavassa T., 2012, AJ, 756, 11
Danger G., Rimola A., Abou Mrad N., Duvernay F., Roussin G., Theulé P., Chiavassa T., 2014, Phys. Chem. Chem. Phys., 16, 3360
Dovesi R. et al., 2009, CRYSTAL09 User's Manual. Univ. Torino, Torino
Duvernay F., Dufauret V., Danger G., Theulé P., Borget F., Chiavassa T., 2010, A&A, 523, A79
Elsila J. E., Dworkin J. P., Bernstein M. P., Martin M. P., Sandford S. A., 2007, AJ, 660, 911
Fresneau A., Danger G., Rimola A., Theulé P., Duvernay F., Chiavassa T., 2014, MNRAS, 443, 2991
Frisch M. J. et al., 2013, GUASSIAN 09. Gaussian Inc, Wallingford, CT
Gerakines P. A., Moore M. H., Hudson R. L., 2004, Icarus, 170(1), 202
Gerakines P. A., Schutte W. A., Greenberg J. M., Vandishoeck E. F., 1995, A&A, 296, 810
Grimme S., 2010, J. Chem. Phys. Chem. Phys., 132, 154104
Kendall E. C., McKenzie B. F., 1929, Org. Synth., 9, 4
Lee C., Yang W., Parr R. G., 1988, Phys. Rev. B., 37, 785
Lerner N. R., Cooper G. W., 2005, Geochim. Cosmochim. Acta, 69, 2901
McQuarrie D., 1986, Statistical Mechanics. Harper and Row, New York
Noble J. A., Theulé P., Borget F., Danger G., Chomat M., Duvernay F., Mispelaer F., Chiavassa T., 2013, MNRAS, 428, 3262
Perdew J.P., Burke K., Ernzerhof M., 1996, Phys. Rev. Lett., 77, 3865
Rimola A., Sodupe M., Ugliengo P., 2010, Phys. Chem. Chem. Phys., 12, 5285
Schutte W., Allamandola L., Sandford S., 1993, Icarus, 104, 118
Strecker A., 1854, Ann. Chemie Pharm., 91, 349
Vinogradoff V., Rimola A., Duvernay F., Danger G., Theulé P., Chiavassa T., 2012a, Phys. Chem. Chem. Phys., 14, 12309
Vinogradoff V., Duvernay F., Farabet M., Danger G., Theulé P., Borget F., Guillemin J. C., Chiavassa T., 2012b, J. Phys. Chem. A, 116, 2225

This paper has been typeset from a Microsoft Word file prepared by the author.